

# Heme isomers substantially affect heme's electronic structure and function

**Kepp, Kasper Planeta**

*Published in:*
Physical Chemistry Chemical Physics

*Link to article, DOI:*
10.1039/c7cp03285d

*Publication date:*
2017

*Document Version*
Peer reviewed version

**Heme isomers substantially affect heme electronic structure and function**

Kasper P. Kepp*

*Technical University of Denmark, DTU Chemistry, Building 206, 2800 Kgs. Lyngby, DK – Denmark.*

* Corresponding Author. Phone: +045 45 25 24 09. E-mail: kpj@kemi.dtu.dk

## Abstract

Inspection of heme protein structures in the protein data bank reveals four isomers of heme characterized by different relative orientations of the vinyl side chains; remarkably, all these have been reported in multiple protein structures. Density functional theory computations explain this as due to similar energy of the isomers but with a sizable (25 kJ/mol) barrier to interconversion arising from restricted rotation around the conjugated bonds. The four isomers, EE, EZ, ZE, and ZZ, were then investigated as 4-coordinate hemes, as 5-coordinate deoxyhemes, in 6-coordinate $O_2$-adducts of globins and as compound I intermediates typical of heme peroxidases. Substantial differences were observed in electronic properties relevant to heme function: Notably, the spin state energy gap of $O_2$-heme adducts, important for fast reversible binding of $O_2$, depends on isomer state, and $O_2$-binding enthalpies change by up to 16 kJ/mol; redox potentials change by up to 0.2 V depending on isomer, and the doublet-quartet energy splitting of compound I, central to "two-state" reactivity, is affected by up to ~15 kJ/mol. These effects are consistently seen with three distinct density functionals, i.e. the effects are not method-dependent. Thus, the nature of the isomer state is an important but overlooked feature of heme chemistry and function, and previous and future studies of hemes may be reconsidered in this new context.

**Keywords: Heme, isomers, electronic structure, DFT, spin crossover, chemical bonding**

## Introduction

Heme plays a central role in biological matter as the main oxygen manager of oxygenic heterotrophs[1,2] and as a cofactor of oxygen-activating enzymes such as peroxidases, catalases and cytochromes $P_{450}$[3–7] and electron transfer processes involved in bioenergy processes[8,9]. Heme evolved approximately two billion years ago[10]; its electronic structure is delicately tuned to effectuate its various biological functions[2,11], notably providing it with a remarkable reversible redox potential[12], low reorganization energy[13], and spin crossover properties[14–17].

Hemes contain a porphyrin ring with iron bound and different groups attached that give rise to different types of hemes[18,19], the most common being heme B[20]. Heme B has two vinyl side chains in addition to four methyl substituents and two propionate side chains. The vinyl side chains are attached to the aromatic porphyrin ring, and the connecting bonds are conjugated. This may restrict rotation of the vinyl groups, and to a different extent[21]. Additionally, steric clashes between the methyl and vinyl side chains may further restrict rotation. Accordingly, these side chains produce E,Z-type isomerism, with all four isomers shown in Figure 1A, which can affect the function of heme proteins.

Symmetric protohemes III and XIII (where the vinyl groups are either close or separated) show only small effects on the heme function[22]. However, changing the weakly donating vinyl groups into electron-withdrawing formyl groups favors low-spin and changes oxygen affinity[23,24], and other side-chain modifications affect the optical and oxygen binding properties[25,26]. In the context of the protein, these differences are more pronounced, and even the orientation of the heme alone and its relation to the proximal histidine can affect the properties due to the asymmetry of the protein cavity[27–30]. Theoretical studies indicate that side chain modifications can change cytochrome P450 reactivity[31]. All these studies involved direct chemical modifications of the side chains. Apparently, the isomers resulting directly from restricted bond rotation have not been studied before.

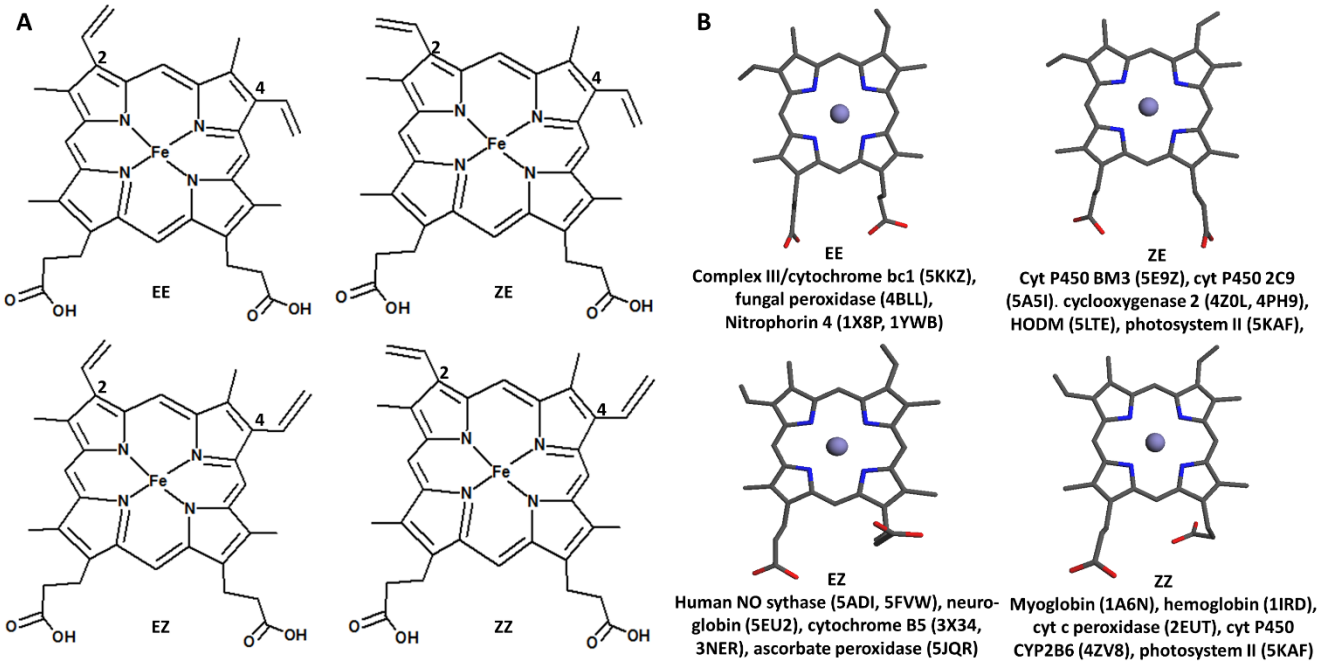


**Figure 1. A)** Four theoretical isomers of heme B, differing by the orientation of the vinyl side chains, with positions 2 and 4 shown. **B)** Examples of each isomer with representative PDB codes from the protein data bank.

To explore this, common heme B protein structures from the protein data bank[32] were inspected and the isomer corresponding to Figure 1A was noted. Remarkably, all four types of isomers were repeatedly identified (Figure 1B). Notably, these are *not* simply orientation isomers formed by the protein. In some cases, isomer structures may result from fitting low-resolution electron densities and decisions during assignment of heme densities of unclear or multiple occupation within the heme cavities, or a mixture of orientation conformations rather than two distinct isomers. However, many structures are of high resolution and there are many examples of each isomer, and thus this heterogeneity warrants investigation. Side chain conformations can influence heme protein structure, stability, and function[18,33], and it was thus suspected that the isomer state can affect electronic structure and perhaps be functionally important; exploring this possibility was the motivation of this work.

## Computational details

**Chemical models.** A variety of models with different coordination modes were studied. To understand the direct influence of the isomer state on the equatorial ligand field of heme, 4-coordinate models of all four isomers the full heme B ring without axial ligands were studied in both high-spin (HS) and low spin (LS) states for both Fe(III) and Fe(II) states (16 systems). The models consisted of the full heme in the four isomer states without any axial ligands; these are referred to as EE0, ZE0, EZ0, and ZZ0. The Fe(II)/Fe(III) states have charges of −2 and −1, respectively. The high-spin Fe(II) states of these models have 163 α-electrons and 159 β-electrons; low-spin has 161 of both types of electrons, Fe(III) high-spin has 163 α-electrons and 158 β-electrons; and low-spin Fe(III) has 161 α- and 160 β-electrons.

In order to relate isomerism to functionality of heme, 6-coordinate models of $O_2$-adducts with imidazole bound as the proximal ligand were also computed in all four states for each of the four isomers (HS and LS Fe(III) and Fe(II), i.e. 16 systems). In addition to the full heme ring these models included a bound $O_2$ molecule at one axial position and an imidazole at the other axial position. For the high-spin Fe(II) states, these models have 193 α-electrons and 189 β-electrons and a charge of −2.

The commonly encountered 5-coordinate deoxyheme state of proteins was also studied by corresponding models for all four isomers; these computations were done both for the ferric and for the more common ferrous HS states. This enabled the computation of the $O_2$-binding enthalpy as the energy of the 6-coordinate $O_2$-adduct minus the energies of the deoxyheme and the triplet $O_2$, corrected for zero point vibrational energies, as discussed further below.

Finally, it was investigated whether the isomer state could also affect compound I, the formally Fe(IV) intermediate coupled to a porphyrin radical, a central intermediate of several heme enzymes such as heme peroxidases. In addition to the full heme ring in the four isomer states, these models included

the ferryl (Fe=O) moiety and a proximal imidazole ligand; these 6-coordinate models were all studied in both the quartet and doublet spin states as these define the electronic structure and function of compound I[34,35]. These models had charges of −1; the quartet states contain 188 α-electrons and 185 β-electrons, whereas the doublet states have 187 and 186 α-and β-electrons.

**Computation of electronic energies.** All computations were performed using the Turbomole software, version 7.0[36]. The resolution of identify approximation[37] was used to speed up calculations throughout this work. The equilibrium geometries of all states described above were optimized using the BP86 functional[38,39] with the def2-SVP basis set[40], a protocol that routinely provides excellent geometries for first row transition metal complexes[41], including porphyrins[15,42] with average errors in metal-ligand bond lengths of 0.02−0.03 Å[41] (electronic energies in Supporting Information Table S1). To describe the energetics in a realistic screened environment, all computations (both geometry optimization and single-point energies with larger basis sets) were carried out with the Cosmo solvent model using a dielectric constant of 10, suitable for the typical screening environment in a heme protein, and using default Cosmo radii for all atoms, and 2.0 Å used for iron.

For accurate single-point energies, a larger triple-zeta valence basis set was applied with inclusion of polarization functions on all atoms including hydrogen atoms (def2-TZVPP)[40]; hydrogen atoms are in close contact in the isomers, and additional polarization functions seem important to ensure electronic freedom at close hydrogen encounters. Dispersion is anticipated to play a significant role for these isomers, and accordingly all energy calculations included dispersion corrections using Grimme's D3 method[43]. To ensure that the changes in structure between isomers were not method-dependent, three functionals were used in parallel for energies: B3LYP[44–46], PBE-D3[43,47], and TPSSh-D3[48,49], with electronic energies converged to $10^{-6}$ a.u. The electronic energies of these computations can be found in Table S2. Accurate energetics of heme have previously been obtained with TPSSh for both spin gaps and binding enthalpies[15,42].

**Zero-point vibrational energies and free energies.** To include the thermodynamic and zero-point energy corrections to the energies and redox potential shifts of the different isomers, the frequencies of all optimized ground states were computed at the same level as geometry optimization, i.e. BP86/def2-SVP. The zero point energies (ZPEs) obtained from these calculations and the enthalpy and vibrational entropy corrections were used to compute free energy estimates for each isomer state using the freeh script of Turbomole at 298 K. The frequencies were scaled by a scale factor of 0.9914 suitable for the applied method (BP86/def2-SVP).

## Results and discussion

**Energy minima and conversion between isomers.** It was suspected that the different isomer states, due to orbital rotation and strain, might display different induction of electron density by the vinyl groups and potentially induce strain in the ring and π-system with associated deviations from co-planarity due to the steric clashes of vinyl and methyl groups. Heme substituents, like other substituents in organic chemistry, can generally be classified as either electron-withdrawing or electron-donating[50]. An electron-withdrawing formyl group in heme A increases the reduction potential by 179 mV[18]. Electron-withdrawing trifluoromethyl groups also affect the $O_2$-binding properties of heme[51]. The propionate side groups are electron-withdrawing, whereas the methyl and vinyl groups are weakly donating. In their totality, the eight substituents of heme B withdraw electron density from the iron center, reduce the isomer shift by ~0.07 mm/s, and increase the Weiss character of the Fe−$O_2$ bond[14]. A similar effect is seen on the isomer shift of deoxyheme[42]. Thus, the heme substituents affect the relative prominence of Fe(III) over Fe(II)[18] and hence back-bonding, reversible binding and reversible binding and activation of $O_2$. It was thus speculated that even the isomer state that reflects steric distortions of such electron induction effects, may affect the properties and function of heme.

To identify the energy scale of conversion between these isomers, the relaxed energy profiles for rotation of the torsion angle of 2-vinyl and 4-vinyl in the ZE0 model that converts between the isomers were computed (Figure 2). The minima are in the vicinity of those for a normal conjugated C−C bond (i.e. 0° and 180°) but importantly deviate from these values due to the steric clashes of the methyl and vinyl groups. Interestingly, rotation involves a double well at –30° and +30° due to this steric clashing. For the 4-vinyl group (Figure 2A), the other minimum is steep and skewed at 195° corresponding to the highly constrained ZZ isomer, or for the 2-vinyl group (Figure 2B) shallow due to weak steric clashing at 150–210°, corresponding to the EE isomer. The isomers interconvert on an energy scale of ~25 kJ/mol regardless of the type of rotation, i.e. they are stable in their separate isomer states; this barrier is probably even higher in proteins due to conformational restriction.

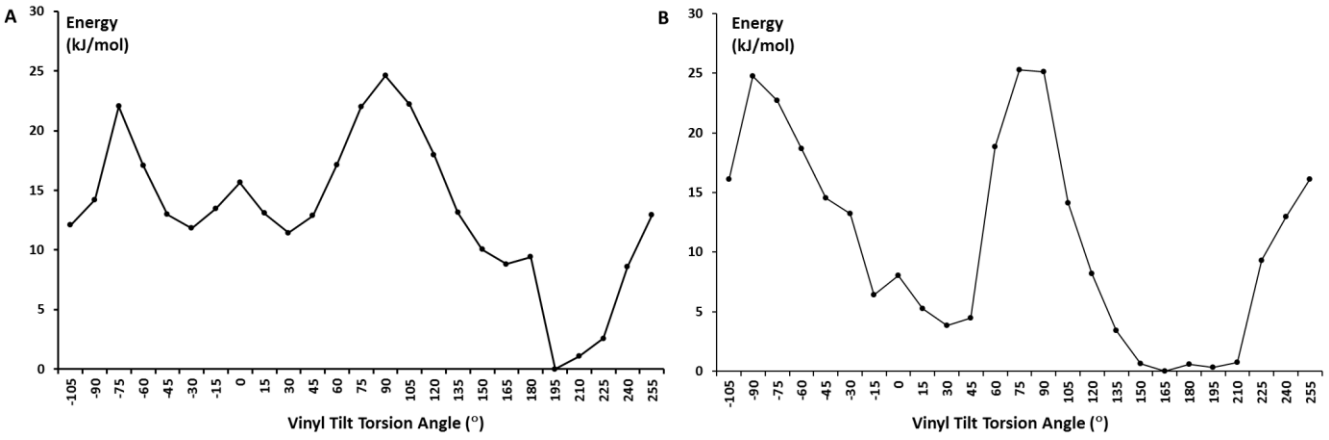


**Figure 2.** Energy profile (TPSSh/def2-TZVPP, Cosmo, ε = 10) of planar heme B for rotation of A) the 4-vinyl and B) the 2-vinyl group of ZE0. The lowest (ZZ) isomer state is steep at 195° (A) or shallow (EE) at 150-210° (B), with a bimodal secondary energy minimum at +30°, –30°; the deviation from smooth curves and from 0° and 180° minima reflects strain from interaction with the methyl substituents.

The def2-TZVPP energies show that the isomers are of similar energy to within 10 kJ/mol (Supporting Information, Figure S1 and Table S3) with only a few exceptions. The EE isomer is generally the least stable, whereas the ZZ isomer is typically most stable, although this depends somewhat on the specific electronic state and coordination mode. EZ and ZE are generally of similar stability within 5 kJ/mol, as perhaps expected because they experience similar strain (Figure 1). For the $O_2$-adducts, the isomer state is interestingly having a larger effect, with the ZZ isomer favored by up to 35 kJ/mol in some distinct electronic spin and redox states, but these are exceptions. Given the combination of similar thermodynamic stability with barriers for interconversion of ~25 kJ/mol, one expects that all four isomers will be functionally important in heme proteins unless the protein precludes some of them by steric control. These observations are robust to the choice of density functional (Table S3). These are isodesmic reactions, making the energy estimates more accurate than typical computational chemistry[52].

Because the energies are similar the isomers will be thermodynamically accessible but kinetically stable and thus play a role in real proteins. Although this work deals with effects of isomers on function, the isomer could also affect the stability of a heme protein, because the heme side chain conformations interacting with the remaining protein play a major role in the critical unfolding step of myoglobin[33,53,54]; although the stability of each isomer needs to be studied by extensive molecular dynamics of unfolding the holoprotein, the stabilization would hardly exceed the 25 kJ/mol of Figure 2, corresponding to full investment of the energy difference of the isomers into protein folding energy, yet this energy would imply that the choice of isomer could substantially affect heme protein stability.

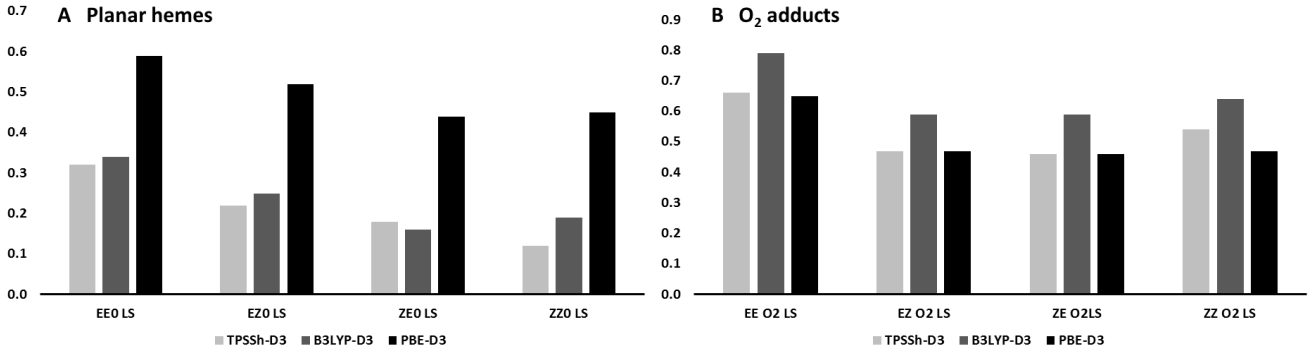


**Figure 3.** Computed half reduction potentials Fe(III)heme + $e^- \rightarrow$ Fe(II)heme (vs. SHE) for isomers of **A)** planar hemes and **B)** $O_2$-adducts from TPSSh-D3, B3LYP-D3, and PBE-D3 (def2-TZVPP, Cosmo).

**Isomer states change redox potentials by up to 0.2 V.** To investigate whether the identified isomers of heme in real protein structures have any functional consequences, the standard reduction potentials of the half reaction Fe(III)heme + $e^- \rightarrow$ Fe(II)heme was computed for all isomers in both the planar 4-coordinate heme B and in the 6-coordinate $O_2$-adduct (Figure 3; numerical data in Supporting Information, Table S4). The potentials were corrected by the experimental potential of the hydrogen electrode (4.44 V) to put them on a chemically relevant scale; however, this does not affect the relative potentials, due to the cancellation of the absolute potential reference. Accordingly, while the absolute potentials computed with the different methods vary substantially as expected, the relative potentials are consistently reproduced. The isodesmic comparison is more accurate than typical non-isodesmic computational chemistry because the same orbital occupations and general electronic structures are involved and errors in describing these cancel out during subtraction of electronic energies for different isomers when computing the potential shift due to isomer state; differential dispersion, strain and induction effects due to vinyl group orientations largely produce these shifts.

Figure 3 shows that all three methods produce the highest potential for the EE isomers with both coordination numbers. For the planar heme, the EZ isomer has the second-highest potential ~0.1 V below EE, whereas the ZE and ZZ isomers have the lowest, similar potentials, about 0.15–0.2 V lower than EE. For the 6-coordinate hemes, all the three isomers EZ, ZE, and ZZ have similar potentials that are approximately 0.2 V lower than the EE isomer. Thus, the EE isomer and to some extent the 4-coordinate EZ isomer have distinctly higher half potentials than the other isomers, which should probably be accounted for when studying hemes and heme proteins more generally. The EE isomer is distinct by having the smallest amount of strain energy because both vinyl groups point away from their neighbor methyl groups. This structure preserves the electron-withdrawing capability of the propionates, causing the higher half potential of EE isomers, an effect that is largely independent of the coordination number of heme.

**$O_2$-adduct electronic structure is affected by isomer state.** One of the most important structures of life is the $O_2$-adduct of heme, responsible for carrying $O_2$ in animals, and a common early intermediate in $O_2$-activating heme enzymes. The adduct is characterized by the extent of back-bonding of iron d-electron density into $\pi^*$ orbitals on $O_2$[15], with a vibration wave number for the O−O bond close to 1100 $cm^{-1}$ of superoxide[55], reflecting a balance between Pauling[56] and Weiss[57] character[35,58–60]. The computed equilibrium bond lengths (Table S5, Figure S2) reveal only small differences between the same electronic states of the different isomers and produce the expected increase in Fe–O and Fe–N bond lengths from LS to HS and from ferric to ferrous iron, including the inverse relationship between Fe–O and O–O bonds characteristic of back-bonding. However, the ZZ isomer produces a slightly longer Fe–O bond in the LS ferrous state (Figure S2). This isomer is one of the most commonly assumed and relatively stable overall (Figure S1), and the most stable $O_2$-adduct, Table S3.

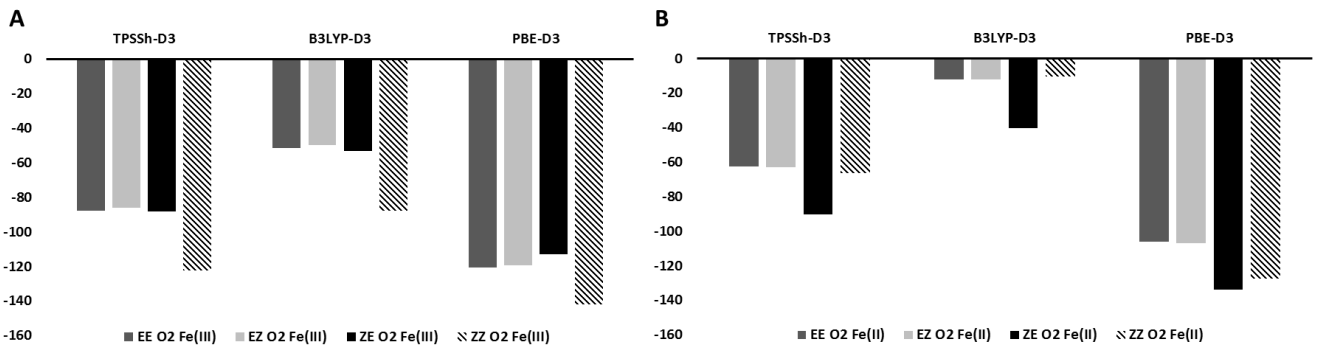


**Figure 4.** Energy difference between high-spin and low-spin states of Heme$O_2$ for the four different isomers: **A)** Fe(III) systems; **B)** Fe(II) systems.

The spin states are central to the reactivity of hemes and are distinctly close-lying[61]. The five-coordinate hemes are typically high-spin whereas the six-coordinate hemes tend to be low-spin[62]; 4-coordinate iron(II)porphyrin has an intermediate spin ground state[63,52]. The ability of heme to reversibly bind $O_2$ depends on the spin-crossover tendencies of heme; the close-lying spin states enable the fast spin inversion required for fast, reversible binding and release in biological tissue[14]. This "broad crossing mechanism"[14] enables spin-forbidden ligand binding where spin orbit coupling is limited to a few kJ/mol[60]. Accordingly, the effect of isomer on the energy difference between HS and LS states is of particular interest. This energy difference was computed for 4- and 6-coordinate models (numerical data in Supporting Information, Tables S6 and S7).

Figure 4A (Fe(III)) and Figure 4B (Fe(II)) show this gap in kJ/mol for the different isomers computed with the three dispersion-corrected functionals. PBE is known to overstabilize the LS state, whereas B3LYP-D3 favors HS and TPSSh-D3 is more well-balanced[15,64]. Yet it is notable that all methods provide similar *relative* effects of the isomers, which shows that these relative effects are robust to method choice. A number of other observations are interesting: 1) Fe(III) favors LS more, as expected from the spectrochemical series of metal ions[65] and corresponding DFT computations[66]; 2) all three

methods agree that for the Fe(III) adduct, the ZZ isomer favors LS more than the other three isomers by 20–30 kJ/mol; this isomer has maximally strained side chain encounters (Figure 1); 3) for the biological ferrous resting state, the ZE isomer surprisingly favors LS more, with the other isomers being similar. The effect on spin gap is of a magnitude that would affect spin crossover probability and thus the rate of binding as quantified previously[14]. The fact that the ZZ isomer favors LS in the ferric state but that ZE favors LS in the ferrous state could bot have been predicted by simple chemical considerations, yet the effect is notable.

**Effect of isomer state on $O_2$ affinity.** The affinity of $O_2$ for heme plays a major role in $O_2$-storage, transport and activation by heme enzymes and is thus a key parameter in understanding heme function[2]. The experimental enthalpy of $O_2$-binding to heme is approximately –59 kJ/mol[67]. It has previously been shown that TPSSh-D3 reproduces this energy accurately whereas GGA functionals such as PBE overbind and B3LYP underbinds and does not predict binding at all[14]. Table 1 shows the energies of binding for TPSSh_D3, B3LYP-D3, and PBE-D3 using the def2-TZVPP basis set and corrected for zero-point energies, calculated as E(oxyheme) – E($O_2$) – E(deoxyheme) + ZPE(oxyheme) – ZPE($O_2$) – ZPE(deoxyheme), where E refers to electronic energies of triplet $O_2$, 5-coordinate deoxyheme, and 6-coordinate oxyheme, whereas ZPE refers to the corresponding zero-point energies (details of these calculations are found in Supporting Information, Tables S10 and S11). The last column of Table 1 shows the computed enthalpies for TPSSh with energies corrected for vibrational and thermal corrections using the vibrational state function, calculated by the freeh module.

As expected from previous work[14,42], B3LYP (even with dispersion included which strengthens binding) fails to predict any binding, PBE-D3 overbinds, and the experimental enthalpy of binding of –59 kJ/mol is best reproduced by TPSSh-D3 (final column of Table 1 after correction for vibration and thermal contributions); with this method, the binding enthalpies agree with experiment within 20 kJ/mol.

Also, because of the isodesmic nature of the comparison across isomer reactions, the *trend* in binding enthalpy for the isomer is not dependent on method choice beyond a few kJ/mol and always give ZZ < EZ < ZE ~ EE, showing that the electronic effect of isomer state on $O_2$-binding is accurate.

For the ZZ isomer, the difference between TPSSh-D3-computed and experimental values is only 5 kJ/mol. This is notable because the ZZ isomer is commonly found in the globins where this process takes place and thus the likely isomer measured experimentally. By itself, the isomer state effects the enthalpy by up to 16 kJ/mol, with other isomers binding $O_2$ less strongly. Interestingly, the isomer state of typical $O_2$-activating heme enzymes is not ZZ as in the $O_2$-transporting globins, but often other isomers that produce weaker $O_2$-binding, according to the present calculations in Table 1; thus the isomer state may play a role in tuning the function of heme between the two scenarios of reversible binding vs. activation of $O_2$ that is much studied in other contexts[2,68].

**Table 1. Computed energies and enthalpies of $O_2$-binding, corrected for zero-point vibrational energies.**

| Isomer | ΔE, TPSSh-D3 (kJ/mol) | ΔE, B3LYP-D3 (kJ/mol) | ΔE, PBE-D3 (kJ/mol) | ΔH, TPSSh-D3 (kJ/mol) |
|---|---|---|---|---|
| EE | –29.3 | 52.7 | –115.3 | –41.1 |
| EZ | –36.6 | 43.1 | –118.7 | –49.2 |
| ZE | –25.7 | 51.7 | –117.5 | –37.9 |
| ZZ | –47.5 | 31.5 | –130.5 | –54.2 |

**Isomer state can affect "two-state" balance of compound I.** Close-lying spin states are also found in compound I and routinely obtained with both DFT and CASPT2 methods[5,34]. In compound I of heme enzymes, the doublet and quartet states are very close in energy[17,69] due to the antiferromagnetic

vs. ferromagnetic coupling of an intermediate spin Fe(IV) with a ligand-based radical[5,17,70]. This radical delocalization facilitates oxygen activation[34,68].

Figure 5A shows the effect of isomer state on the doublet-quartet splitting of compound I (numerical data in Table S8), with a simple d-orbital diagram of ferromagnetic coupling shown in Figure 5B. Again, three cases are similar (EE, ZE, ZZ), with a preference towards the anti-ferromagnetic coupled doublet of ~5 kJ/mol judged from the more accurate TPSSh-D3 and B3LYP-D3 energies, whereas the PBE shifts the energy in favor of the quartet by ~5 kJ/mol (notice that the chemically relevant *shift* in quartet-doublet preference caused by isomer state is consistently produced by all methods). However, the EZ isomer notably favors the ferromagnetic coupled quartet state. The strain interaction of EZ is distinct from that of ZE by the different orientation of the vinyl side chain on the pyrrole ring (Figure 1); it is understandable that this effect can change the stability of the ferromagnetic interaction with the full, conjugated π-system. When the vinyl groups clash with the methyl groups, electron induction changes and the planar π-system experiences peripheral strain. This occur in different places of the ring in the EZ and ZE isomers relative to the carboxylic side chains, i.e. the induction effects and π-strain mix non-trivially. When this effect translates into energy it seen to become functionally relevant for two-state reactivity, with changes in doublet-quartet state preference of up to 15 kJ/mol (Figure 5).

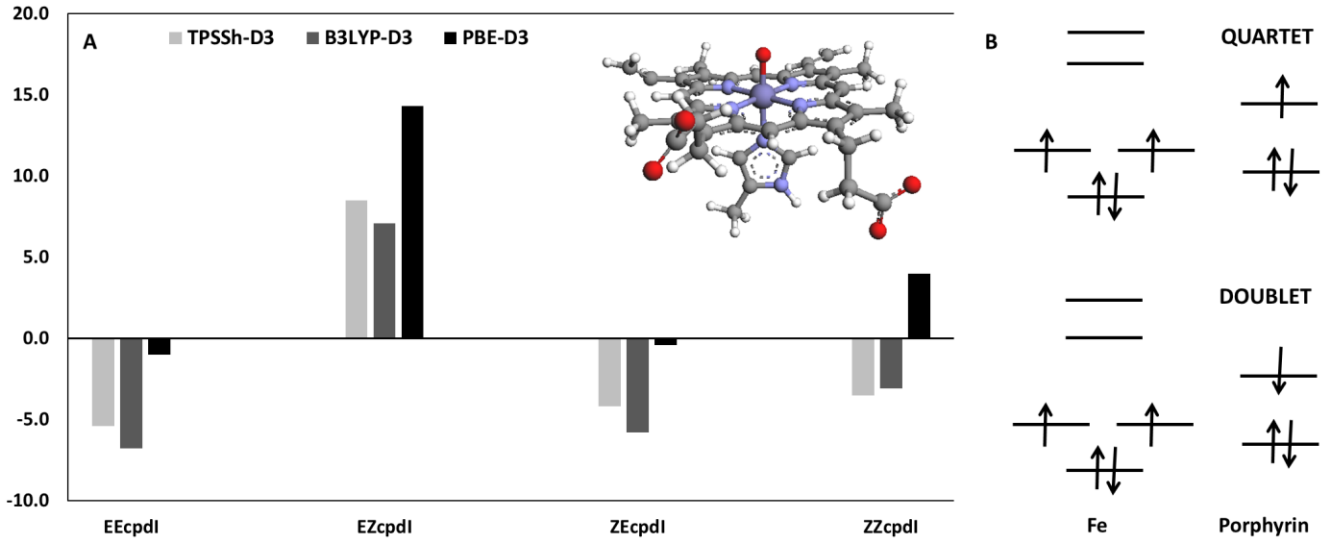


**Figure 5.** Effect of isomer state on doublet-quartet splitting of compound I (energies in kJ/mol). A positive number means that quartet is favored.

**"Transition states" of the isomers observed in experimental structures.** The above computations indicate that it is relevant to account for the isomer state of heme in future studies as it may affect reactivity and stability. The four isomers have been in multiple experimental structures, and the reasons for changing between them are envisioned to inspire future research.

A final discussion is warranted regarding some other configurations of heme seen repeatedly in experimental crystal structures. Notably, examples can be found of heme structures whose torsion angles suggest that they are energy maxima according to Figure 2. These crystal states are not expected to be stable and probably represent averages of two distinct isomers of the types identified and discussed in this work. Some examples of this phenomenon are given in Figure 6: The ZZ/EZ-type transition state can be observed in human heme oxygenase 1 (PDB code: 1N45), human myeloperoxidase (PDB code: 3F9P), and human neuroglobin (PDB code: 4MPM), where the 2- and 4-numbers designate which vinyl group is rotated in the transition state. Examples of double transition states (which would reflect a

compromise between essentially all four isomers) have also been reported; an example being human cytochrome C. Because of the energy differences between isomers and the rotational restriction found in this work (Figure 2) it is unlikely that these representations are realistic, except in special cases where the protein may enforce one or more isomer states for functional purposes. The possibility that the protein may do so by steric control is interesting in light of the present findings and will be explored further in future work.

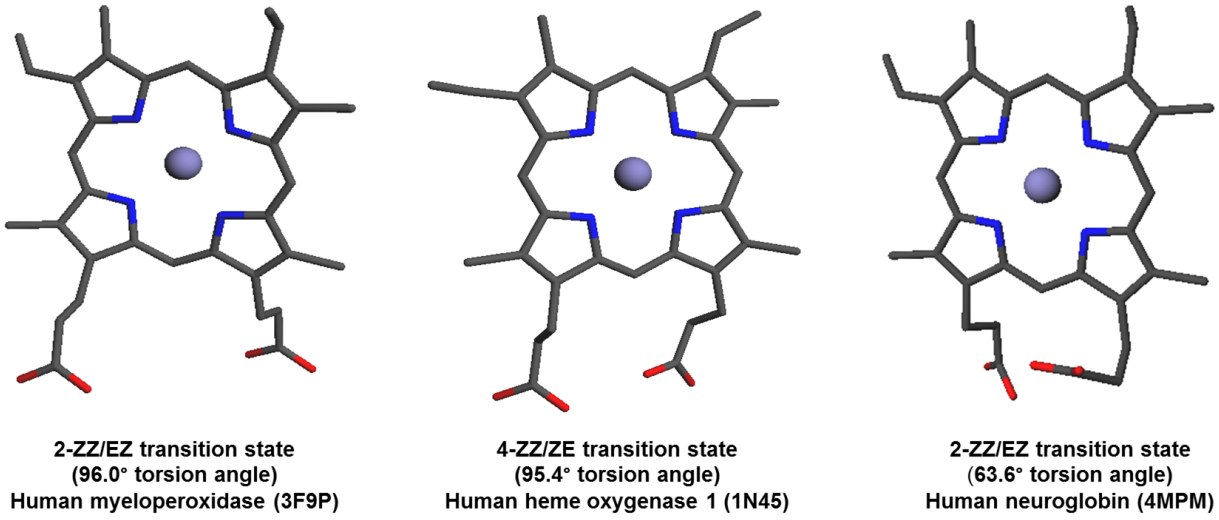


**Figure 6.** Examples of transition states between two isomers reported in crystal structures.

To put into perspective the structural heterogeneity and isomer states discussed in this work, in the new structure from 2016 of photosystem II (5KAF)[71] there is both ZZ heme (101) and ZE heme (201). The significance of this is probably small if this assignment is a coincidental result of the density fitting; however, given the data shown here and the prevalence of all four isomers in other structures, it could be highly relevant that a protein uses multiple isomer states, e.g. for redox potential tuning (with possible benefits up to 0.2 V as suggested above) or for electronic optimization and conversions between involved states, but other roles could also be envisioned.

## Conclusions

It has been shown that experimental heme protein structures contain all four types of isomers defined in Figure 1. The possible functional consequences of these different isomer states have been explored by density functional theory. The induction effects of the methyl and vinyl groups relative to the carboxylic side chains, the wider ring electron density and the distortion of the planar π-system caused by methyl-vinyl steric clashes produce energy effects up to typically 20 kJ/mol or 0.2 V for redox potentials. It is also shown that $O_2$-binding enthalpies varies by up to 16 kJ/mol due to the type of isomer involved in the binding process, which would affect the oxygenation equilibrium of the heme protein. As discussed for some important examples, these energies are large enough to affect heme reactivity and stability. Proteins may further enforce one isomer by steric control. Exploring further the role of isomers in heme proteins thus seems a relevant priority of future studies.

**Supporting information available.** The Supporting Information file includes the electronic energies, zero-point energies from vibration frequency computations, and thermochemical corrections to all computed systems (Table S1); the def2-TZVPP energies with dispersion corrections for TPSSh, B3LYP, and PBE (Table S2); the relative energies of the isomers in kJ/Mol (Table S3); the corresponding energies plotted (Figure S1); the computed half potentials vs. SHE (Table S4); optimized bond lengths (Table S5); histogram of Fe–O and O–O bond lengths in $O_2$-adducts (Figure S2); energy separations between high- and low-spin states for planar hemes (Table S6) and $O_2$-adducts (Table S7); doublet-quartet energy separations for compound I (Table S8); electronic energies (in hartree) for computing relaxed potential energy surfaces (Table S9); electronic energies for geometry optimization and vibration and thermal

corrections for 5-coordinate systems (Table S10); electronic energeis for def2-TZVPP energies of 5-coordinate systems (Table S11).

**Acknowledgements.** The Danish Center for Scientific Computing / Aarhus Supercomputer Center is gratefully acknowledged for providing the computational resources for the project.

**References**

1 T. Yonetani and K. Kanaori, *Biochim. Biophys. Acta*, 2013, **1834**, 1873–1884.

2 K. P. Kepp, *Coord. Chem. Rev.*, 2017, **344**, 363–374.

3 M. Sono, M. P. Roach, E. D. Coulter and J. H. Dawson, *Chem. Rev.*, 1996, **96**, 2841–2888.

4 A. Wilks and G. Heinzl, *Arch. Biochem. Biophys.*, 2014, **544**, 87–95.

5 B. Meunier, S. P. de Visser and S. Shaik, *Chem. Rev.*, 2004, **104**, 3947–3980.

6 T. L. Poulos, *Chem. Rev.*, 2014, **114**, 3919–3962.

7 I. G. Denisov, T. M. Makris, S. G. Sligar and I. Schlichting, *Chem. Rev.*, 2005, **105**, 2253–2277.

8 J. G. Kleingardner and K. L. Bren, *Acc. Chem. Res.*, 2015, **48**, 1845–1852.

9 S. Yoshikawa and A. Shimada, *Chem. Rev*, 2015, **115**, 1936–1989.

10 R. C. Hardison, *Proc. Natl. Acad. Sci. U. S. A.*, 1996, **93**, 5675–5679.

11 P. S. de Visser and J. M. Stillman, *Int. J. Mol. Sci.* , 2016, 17.

12 J. S. Valentine, R. P. Sheridan, L. C. Allen and P. C. Kahn, *Proc. Natl. Acad. Sci.* , 1979, **76**,

1009–1013.

13 P. Rydberg, E. Sigfridsson and U. Ryde, *J. Biol. Inorg. Chem.*, 2004, **9**, 203–223.

14 K. P. Kepp, *ChemPhysChem*, 2013, **14**, 3551–3558.

15 K. P. Kepp, *J. Inorg. Biochem.*, 2011, **105**, 1286–1292.

16 T. Ikeue, Y. Ohgo, T. Yamaguchi, M. Takahashi, M. Takeda and M. Nakamura, *Angew. Chemie Int. Ed.*, 2001, **40**, 2617–2620.

17 S. P. de Visser, *J. Phys. Chem. A*, 2005, **109**, 11050–11057.

18 J. Zhuang, A. R. Reddi, Z. Wang, B. Khodaverdian, E. L. Hegg and B. R. Gibney, *Biochemistry*, 2006, **45**, 12530–12538.

19 T. Mogi, K. Saiki and Y. Anraku, *Mol. Microbiol.*, 1994, **14**, 391–398.

20 M. Kotani, *Ann. N. Y. Acad. Sci.*, 1969, **158**, 20–49.

21 J. Hudeček, P. Hodek, E. Anzenbacherová and P. Anzenbacher, *Biochim. Biophys. Acta (BBA)-General Subj.*, 2007, **1770**, 413–419.

22 Y. Mie, C. Yamada, G. P.-J. Hareau, S. Neya, T. Uno, N. Funasaki, K. Nishiyama and I. Taniguchi, *Biochemistry*, 2004, **43**, 13149–13155.

23 M. Sono and T. Asakura, *J. Biol. Chem.*, 1976, **251**, 2664–2670.

24 M. Sono and T. Asakura, *J. Biol. Chem.*, 1975, **250**, 5227–5232.

25 K. Kawabe, K. Imaizumi, K. Imai, I. Tyuma, H. Ogoshi, T. Iwahara and Z. Yoshida, *J. Biochem.*, 1982, **92**, 1703–1712.

26 S. Neya, M. Nagai, S. Nagatomo, T. Hoshino, T. Yoneda and A. T. Kawaguchi, *Biochim. Biophys. Acta*, 2016, **1857**, 582–588.

27 M. Nagai, Y. Nagai, Y. Aki, K. Imai, Y. Wada, S. Nagatomo and Y. Yamamoto, *Biochemistry*, 2008, **47**, 517–525.

28 F. Rwere, P. J. Mak and J. R. Kincaid, *Biopolymers*, 2008, **89**, 179–186.

29 Q. Peng, M. Li, C. Hu, J. W. Pavlik, A. G. Oliver, E. E. Alp, M. Y. Hu, J. Zhao, J. T. Sage and W. R. Scheidt, *Inorg. Chem.*, 2013, **52**, 11361–11369.

30 A. S. Galstyan, S. D. Zarić and E.-W. Knapp, *J. Biol. Inorg. Chem.*, 2005, **10**, 343–354.

31 J. E. Mendieta-Wejebe, M. C. Rosales-Hernández, H. Rios, J. Trujillo-Ferrara, G. López-Pérez, F. Tamay-Cach, R. Ramos-Morales and J. Correa-Basurto, *J. Mol. Model.*, 2008, **14**, 537–545.

32 H. M. Berman, J. Westbrook, Z. Feng, G. Gilliland, T. N. Bhat, H. Wessig, I. N. Shindyalov and P. E. Bourne, *Nucleic Acids Res*, , DOI:10.1093/nar/28.1.235.

33 M. S. Hargrove and J. S. Olson, *Biochemistry*, 1996, **35**, 11310–11318.

34 E. Derat and S. Shaik, *J. Am. Chem. Soc.*, 2006, **128**, 8185–8198.

35 S. Shaik and H. Chen, *J. Biol. Inorg. Chem.*, 2011, **16**, 841–855.

36 R. Ahlrichs, M. Bär, M. Häser, H. Horn and C. Kölmel, *Chem. Phys. Lett.*, 1989, **162**, 165–169.

37 K. Eichkorn, O. Treutler, H. Öhm, M. Häser and R. Ahlrichs, *Chem. Phys. Lett.*, 1995, **240**, 283–290.

38 A. D. Becke, *Phys. Rev. A*, 1988, **38**, 3098–3100.

39 J. P. Perdew, *Phys. Rev. B*, 1986, **33**, 8822–8824.

40 F. Weigend and R. Ahlrichs, *Phys. Chem. Chem. Phys.*, 2005, **7**, 3297–3305.

41 K. P. Jensen, B. O. Roos and U. Ryde, *J. Chem. Phys.*, 2007, **126**, 14103.

42 K. P. Kepp and P. Dasmeh, *J. Phys. Chem. B*, 2013, **117**, 3755–3770.

43 S. Grimme, J. Antony, S. Ehrlich and H. Krieg, *J. Chem. Phys.*, 2010, **132**, 154104.

44 A. D. Becke, *J. Chem. Phys.*, 1993, **98**, 5648–5652.

45 C. Lee, W. Yang and R. G. Parr, *Phys. Rev. B*, 1988, **37**, 785.

46 P. J. Stephens, F. J. Devlin, Cf. Chabalowski and M. J. Frisch, *J. Phys. Chem.*, 1994, **98**, 11623–11627.

47 J. P. Perdew, K. Burke and M. Ernzerhof, *Phys. Rev. Lett.*, 1996, **77**, 3865.

48 J. Tao, J. P. Perdew, V. N. Staroverov and G. E. Scuseria, *Phys. Rev. Lett.*, 2003, **91**, 146401.

49 J. P. Perdew, J. Tao, V. N. Staroverov and G. E. Scuseria, *J. Chem. Phys.*

50 T. G. Spiro, A. V Soldatova and G. Balakrishnan, *Coord. Chem. Rev.*, 2013, **257**, 511—527.

51 T. Shibata, E. Furuichi, K. Imai, A. Suzuki and Y. Yamamoto, *J. Porphyr. Phthalocyanines*, 2015, **19**, 301–307.

52 K. P. Kepp, *Coord. Chem. Rev.*, 2013, **257**, 196–209.

53 P. Dasmeh and K. P. Kepp, *PLoS One*, 2013, **8**, e80308.

54 M. S. Hargrove, A. J. Wilkinson and J. S. Olson, *Biochemistry*, 1996, **35**, 11300–11309.

55 J. P. Collman, J. I. Brauman, T. R. Halbert and K. S. Suslick, *Proc. Natl. Acad. Sci.*, 1976, **73**, 3333–3337.

56 L. Pauling, *Nature*, 1964, **203**, 182–183.

57 J. J. Weiss, *Nature*, 1964, **202**, 83–84.

58 K. P. Jensen, B. Roos and U. Ryde, *J. Inorg. Biochem.*, 2005, **99**, 45–54.

59 H. Chen, M. Ikeda-Saito and S. Shaik, *J. Am. Chem. Soc.*, 2008, **130**, 14778–14790.

60 K. P. Jensen and U. Ryde, *J. Biol. Chem.*, 2004, **279**, 14561–14569.

61 P. George, J. Beetlestone and J. S. Griffith, *Rev. Mod. Phys.*, 1964, **36**, 441.

62 W. R. Scheidt and C. A. Reed, *Chem. Rev.*, 1981, **81**, 543–555.

63 T. Kitagawa and J. Teraoka, *Chem. Phys. Lett.*, 1979, **63**, 443–446.

64 K. P. Kepp, *Inorg. Chem.*, 2016, **55**, 2717–2727.

65 C. K. Jørgensen, *Mol. Phys.*, 1959, **2**, 309–332.

66 S. R. Mortensen and K. P. Kepp, *J. Phys. Chem. A*, 2015, **119**, 4041–4050.

67 T. G. Traylor and A. P. Berzinis, *Proc. Natl. Acad. Sci.* , 1980, **77**, 3171–3175.

68 K. P. Jensen and U. Ryde, *Mol. Phys.*, 2003, **101**, 2003–2018.

69 D. Sahoo, M. G. Quesne, S. P. de Visser and S. P. Rath, *Angew. Chemie Int. Ed.*, 2015, **54**, 4796–4800.

70 D. L. Harris, J.-Y. Park, L. Gruenke and L. Waskell, *Proteins*, 2004, **55**, 895–914.

71 I. D. Young, M. Ibrahim, R. Chatterjee, S. Gul, F. D. Fuller, S. Koroidov, A. S. Brewster, R. Tran, R. Alonso-Mori, T. Kroll, T. Michels-Clark, H. Laksmono, R. G. Sierra, C. A. Stan, R. Hussein, M. Zhang, L. Douthit, M. Kubin, C. de Lichtenberg, L. Vo Pham, H. Nilsson, M. H.

Cheah, D. Shevela, C. Saracini, M. A. Bean, I. Seuffert, D. Sokaras, T.-C. Weng, E. Pastor, C. Weninger, T. Fransson, L. Lassalle, P. Bräuer, P. Aller, P. T. Docker, B. Andi, A. M. Orville, J. M. Glownia, S. Nelson, M. Sikorski, D. Zhu, M. S. Hunter, T. J. Lane, A. Aquila, J. E. Koglin, J. Robinson, M. Liang, S. Boutet, A. Y. Lyubimov, M. Uervirojnangkoorn, N. W. Moriarty, D. Liebschner, P. V Afonine, D. G. Waterman, G. Evans, P. Wernet, H. Dobbek, W. I. Weis, A. T. Brunger, P. H. Zwart, P. D. Adams, A. Zouni, J. Messinger, U. Bergmann, N. K. Sauter, J. Kern, V. K. Yachandra and J. Yano, *Nature*, 2016, **540**, 453–457.